Journal Name

ARTICLE

Correlating the effective work function at buried organic/metal interfaces with organic solar cell characteristics

Received 00th January 20xx,
Accepted 00th January 20xx

DOI: 10.1039/x0xx00000x

www.rsc.org/

Basel Shamieh[a], Ana S. Anselmo[b,c], Uwe Vogel[b,c], Eirini Lariou[d], Sophia C. Hayes[d], Norbert Koch[b,c], and Gitti L. Frey*[a]

The energy level alignment at organic semiconductor/metal interfaces determines the efficiency of charge injection and collection in organic electronic devices. Back electrodes, applied after the organic layer is processed, form buried organic/metal interfaces that are not directly experimentally accessible for measuring level alignment. Here we devise an approach to evaluate the effective work function (EWF) between an organic solar cell bulk heterojunction (BHJ) and silver electrodes, including interlayers, and correlate the EWF with solar cell characteristics. The platform used are self-generated interlayers formed by migration of additives from the BHJ to the organic/metal interface. The EWFs of interlayer/Ag interfaces are assessed by step-depositing silver on interlayer films followed by in-situ ultraviolet photoelectron spectroscopy and compared with EWF values of the bare Ag/BHJ interface. Solar cell characteristics of devices comprising the same interfaces confirm unambiguously the correlation between EWF and V_{oc}. We stress that the metal work function is a surface property and cannot be reliably used to estimate the energy level alignment at organic/metal buried interfaces. Rather, EWF values should be used to assess the interfacial level alignment. Known EWF values for organic/metal interfaces with and without interlayers can reveal the contribution of the interlayer to device performance.

Introduction

Organic electronics is emerging as a promising technology for novel efficient, flexible, and low-cost applications.[1] The advantages of organic semiconductors compared to their inorganic counterparts, include material property design through chemical synthesis, simple processability, good scalability, and low-power operation.[2, 3] All organic electronic devices, regardless of the application, comprise interfaces for charge injection or extraction between electrodes (most commonly a metal) and the organic active layer. Charge transfer across the organic/metal interface depends on the interfacial electronic energy level alignment. Large energy offsets between the hole and electron conducting states of the organic semiconductors and the metal Fermi level (EF) impose barriers for charge injection, and are detrimental also for charge extraction due to notable contact resistance.[4, 5] Adjusting the level alignment at organic semiconductor/metal interfaces is difficult because it requires simultaneously controlling the morphology and composition of the organic layers near the metal, accounting for chemical interactions (if occurring), and other physico-chemical phenomena, such as the "push-back" effect and interdiffusion.[6-8] A method to alter the level alignment is to introduce ultrathin interlayers, mostly of organic or inorganic compounds, between the organic semiconductor and the metal.[9] Some of the materials employed as interlayers modify the work function of the metal, which results in a different alignment of the frontier organic semiconductor's energy levels.[10, 11]

Interlayers play a key role for the function and efficiency of organic devices and are currently intensively investigated, particularly in organic solar cells (OSCs) with the aim of increasing the power conversion efficiency (PCE).[11-13] In OSCs, reducing the Schottky barriers at the organic/metal interfaces increases the built-in potential within the device and hence device performance.[5, 14] More specifically, proper adjustment of the energy levels at the organic/metal interfaces can increase the short circuit photocurrent (J_{sc}), the open circuit voltage (V_{oc}), and the fill factor (FF).[15, 16] This can be achieved by judicious selection of electrode and interlayer material. Specifically, the top contact in conventional architecture devices (cathode) should be a low work function metal suitable for electron collection from the organic electron acceptor's lowest unoccupied level, i.e., lowest unoccupied molecular orbital (LUMO) level or conduction band edge. However, such metals are inherently prone to oxidation and hence feature low environmental stability.[17] Cathodes with higher work function, although environmentally stable, lead to higher Schottky barriers and thus higher contact resistance, which limits device performance.[15, 18] Therefore, introducing interlayers that reduce the barrier without jeopardizing the environmental stability are needed.[9]

Recently, we demonstrated a significant enhancement in device performance by spontaneously generated interlayers at

[a] Department of Materials Science and Engineering, Technion – Israel Institute of Technology, Haifa, Israel.
[b] Humboldt-Universität zu Berlin, Institut für Physik & IRIS Adlershof, Newtonstrasse 15, 12489, Berlin, Germany.
[c] Helmholtz-Zentrum Berlin für Materialien und Energie, Albert-Einstein-Strasse 15, 12489 Berlin, Germany.
[d] Department of Chemistry, University of Cyprus, P.O. Box 20357, 1678, Nicosia, Cyprus.

Electronic Supplementary Information (ESI) available: [details of any supplementary information available should be included here]. See DOI: 10.1039/x0xx00000x

This journal is © The Royal Society of Chemistry 20xx

Please do not adjust margins

the buried organic/Al or Ag interface.[19-22] This self-generated interlayer formation process, where an additive is mixed with the active organic semiconductor solution, reduces the need for an additional processing step, and it is compatible with roll-to-roll processing, and most importantly, allows tuning of an interface that is generally inaccessible.[21] The key step here is additive migration towards the organic/metal interface, driven by additive-metal interaction during electrode deposition.[23] This process depends on the strength of the interaction versus other factors, such as the size of the additive, the properties of the organic semiconductor, interactions with the bottom substrate, additive surface-energy, and others.[19, 22] Because additive-metal interactions generate the interlayer, and not organic/air surface energy considerations, [24] accumulation of the additive at the organic/metal interface directly improves interfacial charge carrier transfer and hence OSC performance.[19, 21] Therefore, such self-generated interlayers in organic solar cells, provide a unique platform to study the interfacial energy level alignment between an organic semiconductor and metal electrode induced by the interlayer, in correlation with OSC device performance.

Characterizing the electronic structure of interlayers deposited on metal contacts is rather straightforward with using photoemission spectroscopy or Kelvin probe, prior to the deposition of the active organic layer. By measuring the sample work function and valence electronic structure of the subsequently deposited organic layer one can assess the interfacial energy level alignment.[6, 7, 15, 25] However, the changes occurring at organic/metal interfaces upon additive migration towards the metal during and after top metal layer deposition, as considered here, are notoriously difficult to investigate with surface sensitive methods. The valence electron levels of the organic active layer cannot be measured once a few nm of metal are deposited on top due to the short inelastic mean free path of electrons in solids at the photon energies typically used, i.e., a few Å.[26] Furthermore, the work function is, by definition, a surface property and has not simple relation with the energetics inside a solid, and one might refer to the analogon at a buried interface as “effective work function” (EWF). Note, the term EWF as used here and in previous reports refers to properties of a buried interface, while the term work function is only meaningful for a surface.[27] Photoemission and Kelvin probe can thus not directly capture EWF changes of a buried interface.

One approach to overcome this experimental hurdle, Guerrero et al. used Kelvin probe in conjunction with Mott-Schottky analysis of capacitance-voltage measurements to infer the electronic alignment at the buried organic/metal interface.[28] They identified a net charge transfer between the cathode and the organic blend which imposes an interfacial dipole, and depends on the organic surface composition, morphology and type of metal. This observation points to the importance of experimentally accessing the electronic equilibration after organic/cathode interface formation to fully understand its contribution to the photovoltaic performance.[8]

In the present study, we use two different self-generated interlayers to evaluate the EWF at the buried organic/metal interface, which normally form only after metal top contact deposition, and correlate it with device characteristics. To do so, we chose the stable and reproducible OSC working-horse donor:acceptor bulk heterojunction (BHJ) blend poly(3-hexylthiophene-2,5-diyl)(P3HT):phenyl-C61-butyric acid methyl ester (PCBM) (Figure 1 a and b, respectively). The two additives are hexa(ethyleneglycol)-dithiol (HEG-DT) and 1,4-benzenedimethanethiol (BDMT), both thiol-terminated and known to form interlayers in combination with Ag.[20, 29, 30] Silver step-wise deposition onto additive films followed by X-ray photoemission spectroscopy (XPS) confirms additive/silver interactions, and ultraviolet photoelectron spectroscopy (UPS) reveals the corresponding EWF values for Ag coverage that are low enough to not yet exhibit the bare Ag surface properties. For comparison, the EWF of interfacial Ag/P3HT:PCBM without interlayers was also determined. The same additives and additive mixtures are blended into P3HT:PCBM solutions and spun into films. During deposition of the back Ag contact, the additives migrate to the organic/Ag interface to self-generate interlayers. The effect of interlayer formation on the BHJ and the near-interface molecular conformation is studied using surface enhanced resonance Raman spectroscopy (SERRS). Organic solar cell devices, comprising the same types of interfaces used for EWF measurements, allow us to correlate V_{oc} and FF with the interfacial energy level alignment induced by each interlayer.

Experimental

Materials

P3HT (4002-EE, regioregularity 91-94%) was purchased from Rieke Metals; PCBM from Nano-C, and poly(3,4-ethylenedioxythiophene):polystyrene sulfonic acid (PEDOT:PSS) from Haraeus (Clevios PVP AL 4083) and filtered through a 0.22 µm poly(tetrafluoroethylene) (PTFE) filter before use. Hexa(ethyleneglycol)-dithiol (HEG-DT) Mw=314.5 g mol^{-1} and 1,4-benzenedimethanethiol (BDMT) Mw=170.3 g mol^{-1} were purchased from Sigma Aldrich. All materials were used as received.

Organic film deposition and characterization

Defined amounts of either HEG-DT or BDMT were dissolved in 1,2-dichlorobenzene (DCB) and added to a P3HT:PCBM (40:40 mg ml^{-1}) solution in DCB to obtain a series of P3HT:PCBM (20:20 mg ml^{-1}) solutions with 0, 0.25, 0.5, 1, 1.5, 1.75 and 2 mg ml^{-1} of each additive. For additive mixtures, appropriate amounts of HEG-DT and BDMT were mixed together and added to P3HT:PCBM (40:40 mg ml^{-1}) to obtain a series of P3HT:PCBM (20:20 mg ml^{-1}) solutions with HEG-DT:BDMT concentration of 1.75:0.25, 1.5:0.5, 1:1, 0.5:1.5 and 0.25:1.75 mg ml^{-1}. All active

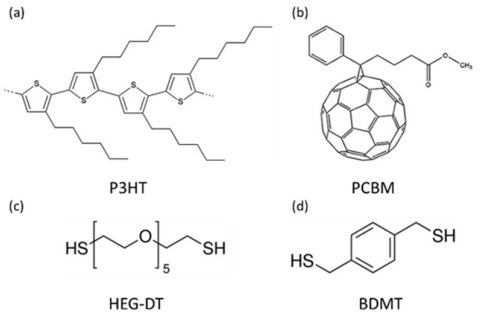

Figure 1: Chemical structures of the compounds studied: (a) P3HT, (b) PCBM, (c) HEG-DT and (d) BDMT.

This journal is © The Royal Society of Chemistry 20xx

Please do not adjust margins

Please do not adjust margins

layers were spun at 1500 rpm for 20 seconds onto PEDOT:PSS/ITO substrates.

Photoelectron Spectroscopy

Photoemission measurements were performed in a custom multi-chamber system using MgKα radiation for XPS and He I from a discharge source for UPS. Photoemission spectra were recorded with a Phoibos 150 (Specs) hemispherical analyzer, with a resolution of 1 eV in XPS and 0.15 eV in UPS. To record the secondary electron cut-off (SECO) for work function determination a bias of -10 V was applied to the sample to clear the analyser work function. The base pressure in the analysis chamber was < 10^{-9} mbar. Samples were prepared in a nitrogen-filled glove box and transferred into the analysis chamber without exposure to air. Ag was evaporated from an electron beam evaporator in the interconnected preparation chamber, at a pressure below 10^{-8} mbar. The nominal deposition rate was monitored with a quartz crystal microbalance; the nominal Ag film thickness values given below do not account for possible differences in sticking coefficient and growth mode between quartz and the samples.

Surface Enhanced Resonance Raman Spectroscopy (SERRS)

The samples were excited at 473 nm with a CW diode laser (Ultralasers, 50 mW OEM DPSS Laser). Samples were measured under vacuum, employing low excitation powers (<0.8mW) to avoid photodegradation. Films were placed such that the excitation beam light passes first through the substrate, facilitating access to the silver/polymer interface. Resonance Raman spectra were also obtained for comparison by exciting the sample again through the substrate but accessing areas without silver. Samples studied here consist of a 3 nm thick silver patch deposited on a glass substrate and topped with active layers of P3HT (20 mg ml^{-1}), P3HT:PCBM (20:20 mg ml^{-1}), P3HT:PCBM:additive (20:20:5 mg ml^{-1}), or a bilayer of concentrated additive topped with P3HT:PCBM (20:20 mg ml^{-1}). The Raman scattered light was collected in a 135o backscattering geometry and delivered to a 0.75 m focal-length Czerny–Turner spectrograph (SpectraPro, SP2760i, Princeton Instruments), equipped with a 1200-grooves/mm UV-enhanced holographic grating. The slit width was set to 100 µm providing for 5 cm−1 spectral resolution. The scattered light was detected by a LN2-cooled 2048×512 pixel, back-illuminated UV-enhanced CCD detector (Spec10:2 KBUV/LN, Princeton Instruments). The spectra were smoothed using Savitzky-Golay filter with a smoothing window of 21 variables and second order polynomials. Cyclohexane was employed for frequency calibration of the spectra.

Device fabrication and characterization

For direct OSCs ITO-covered glass was cleaned by sonication in water, acetone, methanol and isopropyl alcohol. This process was followed by 15 minutes of UV-ozone treatment to remove organic contaminations and activate its surface for enhanced PEDOT:PSS adhesion. PEDOT:PSS was spun at 5000 rpm followed by annealing at 120°C for 15 minutes under ambient conditions. The coated substrates were then transferred into nitrogen atmosphere glovebox for the fabrication process. After deposition of the active layer, a top silver layer was thermally deposited through a shadow mask at a system pressure of ~$4x10^{-6}$ Torr. The thickness of the Ag layer was 100 nm for the devices cathodes directing a device area of 3 mm2. Device characterization was performed in an inert atmosphere under a 100 mW cm^{-2} AM 1.5G class A sun simulator (Science Tech Inc. ss150 solar simulator) using a Keithley 2400 source meter and a labView automated data acquisition program recorded the J-V output. At least 16 devices of each type were measured and the reported values are the average values.

Results and discussion

We employ the self-generated interlayer approach to determine how the EWF at the buried organic/metal interface in OSCs affects device characteristics. To do so, we selected two interlayer-forming additives with similar methane-thiol end groups, but significantly different core, as shown in Figure 1.[20, 31] The backbone of HEG-DT (Figure 1c) is an aliphatic chain while that of BDMT (Figure 1d) is a benzene ring. Therefore, their corresponding interlayers impose distinctly different chemical environments, and hence EWF, at the buried organic/metal interface. Assessing EWF values of the different organic/metal interfaces using photoemission spectroscopy and measuring device characteristics of OSCs comprising the same interfaces will allow us to correlate the EWF of the buried interfaces with device characteristics.[32, 33]

The way to assess how HEG-DT and BDMT as interlayers impact the EWF at interfaces between an Ag electrode and the organic active layer is not as straightforward as directly measuring the evolution of organic semiconductor energy levels on top of a metal electrode as a function of film thickness by UPS, as noted in the introduction. In the latter case, the work function obtained from UPS is indeed representative of the EWF as all changes induced by the organic overlayer are included after monolayer formation. The only exception is energy level bending that occurs when the interface is strongly Fermi level pinned.[34] In the present case, however, the interlayer in devices is formed during and after metal deposition and it is not possible to retrieve EWF once a rather thick Ag layer (several nm) is formed on organic P3HT:PCBM film. The reason is that the work function of a metal is the sum of the bulk chemical potential of electrons inside the metal and the surface dipole, so that once metallic Ag is formed the work function measured does not provide insight into the EWF.[35, 36] Therefore, we devised an approach that should yield the best possible approximation to the energetics inside a device. We form interfaces between the additives and Ag by depositing Ag (sufficiently thin to avoid bulk Ag formation and thus only Ag work function) onto a thin additive layer on a rather inert conductive substrate (indium-tin-oxide), and compare this to additive layers formed directly on Ag thin films. In this way we construct each additive/Ag interface in two opposing ways, which allows assessing plausible EWF values, provided that the Ag overlayers are not too thick and continuous, which would yield only the work function of a bare Ag surface.

This journal is © The Royal Society of Chemistry 20xx

Please do not adjust margins

Please do not adjust margins

We first discuss one interface in detail and then refer to the most important findings for the others. Figure 2 shows UPS and XPS spectra for Ag deposited on a spin-coated layer of HEG-DT supported by ITO. The HEG-DT layer was approximately a monolayer as inferred from evaluation of all core level spectra. Incremental deposition of Ag from one to four nm (nominal coverage) leads to the emergence of a low binding energy component at ca. 162.2 eV in the S 2p spectra (Figure 2a), indicative of the formation of Ag-S-R bonds, as expected. In the spectra of the Ag 3d levels (Figure 2b) we observe that metallic Ag dominates, but as the deposit amount grows, we observe a decrease in a high binding energy (BE) doublet component at ca. 370 eV and 376 eV binding energy, which appears visibly as intensity between the two metallic doublet peaks (at 368.3 eV and 364.3 eV). This high BE component is from Ag that formed bonds with S, but its comparably small intensity shows that metallic island/cluster growth dominates. Notably, the work function of the sample becomes reduced upon Ag deposition (Figure 2c), from 4.05 eV (bare HEG-DT/ITO) to 3.7 eV (1 nm Ag) and it quickly saturates for 2 nm and more at 3.6 eV. This goes in hand with the formation of metallic Ag signatures in the valence region (Figure 2d, also inferred from XPS above), clearly seen by the emergence of the Fermi edge at 0 eV BE. At this stage, we are confident to observe the EWF of the Ag/HEG-DT interlayer, as the work function does not notably vary with Ag deposition and the value is far from that of a thick Ag film (4.15 eV and higher, see Figure 3). Here we note that the work function of a metal surface is not an intrinsic value of the metal, but it depends strongly on the surface structure, specifically the surface electron density distribution. Different crystallographic surface orientations as well as type and density of structural defects let the work function vary be several 100 meV for the same metal.[35, 36] In addition, any adsorbate on the metal, even with low fractional coverage, also impact the work function, in simple physisorptive cases due to the push-back effect.[6-8]

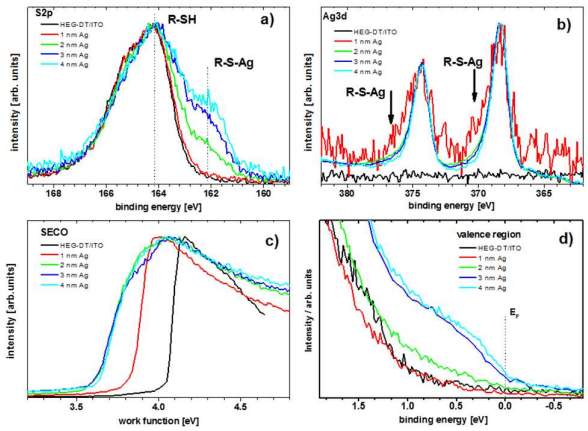

Figure 2: XPS and UPS spectra for incremental Ag deposition onto HEG-DT/ITO. (a) S2p core levels, (b) Ag3d core levels, (c) sample work function from SECO spectra, and (d) valence region close to the Fermi level (E_F).

Experiments analogous to the one described above were performed to assess differences in the EWF of interfaces between the active layer in OSCs (P3HT:PCBM) and Ag electrodes in the presence and absence of HEG-DT, and for comparison, BDMT. The SECO spectra, from which we derive the sample work function show clear trends throughout numerous samples investigated, representative ones are shown in Figure 3. A ca. monolayer film of BDMT spin-cast on ITO exhibits a work function of 4.35 eV (Figure 3a). Upon the deposition of nominal 3 nm Ag, the work function decreases to 4.05 eV. Similarly, the deposition of BDMT from solution onto a pristine Ag film decreases the work function from 4.35 eV to 4.0 eV (Figure 3b). In contrast, the same experimental procedures done with HEG-DT instead of BDMT lead to substantially lower work function values, typically in the range between 3.5 eV and 3.7 eV (Figure 3c and 3d). As these work function values are not representative of a pure Ag surface, they can be regarded as the EWF values relevant at the buried interfaces in OSCs when BDMT and HEG-DT, respectively, form an interlayer between Ag and P3HT:PCBM layer. Finally, to enable comparison of these EWF values with those in an OSC without BDMT and HEG-DT additives, the work function of interfacial Ag/P3HT:PCBM, yet without full Ag coverage, were determined. After deposition of nominal 3 nm Ag onto P3HT-only and mixed P3HT:PCBM, we find a range of work function values, most likely due to interface composition variations from sample to sample as suggested by Guerrero et al.[8] Nonetheless, consistently the estimated EWF values are between 3.6 eV and 4.0 eV (Figure 3e and 3f). Accordingly, we can classify interfaces in terms of EWF values as the highest ones when interfacial BDMT is present (4.05-4.0 eV), followed by interfaces without additive (3.6-4.0 eV), and the lowest values with interfacial HEG-DT (3.5-3.7 eV).

To study the correlation between EWF and V_{oc} we fabricated OSC devices comprising the interfaces used for the photoemission measurements and studied the device characteristics. OSC devices with HEG-DT and BDMT interlayers positioned at the buried interface were prepared by mixing different concentrations of additives into BHJ solutions followed by spin coating active layers onto glass/ITO substrates. As previously reported, the additives migrate to the organic/Ag

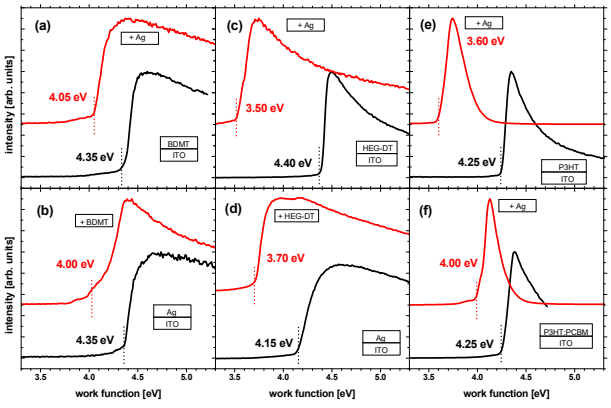

Figure 3: SECO spectra and corresponding work function values of samples before and after the deposition of nominally 3 nm Ag: (a) BDMT on ITO, (c) HEG-DT on ITO, (e) P3HT, and (f) P3HT:PCBM. Before and after deposition of (b) BDMT and (d) HEG-DT on an Ag surface.

This journal is © The Royal Society of Chemistry 20xx

Please do not adjust margins

interface during Ag deposition, generating the interlayers at the buried interface.[20, 23] The driving force for this migration is the interaction between the thiol end-group of the additives and Ag. The extent of additive migration depends on the strength of this interaction versus other factors, such as the size of the additive, the properties of the matrix, interactions with the bottom substrate, the additive's surface-energy, the concentration of additive in the active layer, and temperature. Migration and interlayer accumulation stop once a continuous interlayer is formed at the buried interface.[22]

Current density-voltage (J-V) curves of OSCs incorporating different concentrations of HEG-DT and BDMT are plotted in Figure 4a and b, respectively. The average performance parameters of these devises are listed in Tables 1 and 2. Figure 4c shows the dependence of V_{oc} values on additive concentrations. J-V curves in dark are presented in the supplementary information section Figure S1. First we analyse the performance of devices with a HEG-DT interlayer, Figure 4a. The figure clearly shows that HEG-DT enhances V_{oc} and FF. Similar results were recently reported for self-generated PEG interlayers in P3HT:PCBM devices with Al anodes.[22] It was suggested that the PEG interlayer shifted the "effective work function" of Al tuning the energetics at the interface. Indeed, the V_{oc} and FF increase here are in good agreement with the SECO measurements (Figure 3c and 3d) and EWF estimation above. The EWF obtained for the Ag/HEG-DT interface, 3.5 – 3.7 eV, is lower than the work function of Ag, and hence, introducing HEG-DT at the organic/metal interface reduces the interfacial Schottky barrier and aligns the energy level with the LUMO level of PCBM, ~3.7 eV. Under such conditions, electrons are efficiently transferred between PCBM and the contact.

Analysing the characteristics of devices with BDMT interlayers shows the opposite behaviour to that of devices with HEG-DT interlayers. Figure 4b and Table 2 show that while HEG-DT enhances V_{oc} and FF, BDMT actually reduces both V_{oc} and FF. This result is striking because the EWF value obtained for a buried Ag/BDMT interface, ca. 4.0 eV (Figure 3a and b), is still lower than the work function of Ag. Based on this comparison, a BDMT interlayer should enhance, although moderately, V_{oc} and FF. However, the negative evolution of V_{oc} and FF with BDMT concentration, Figure 4c, unambiguously proves that BDMT increases the energetic misalignment at the interface.

To explain the apparent discrepancy between the EWF value obtained for the BDMT/Ag interface and the worsened device characteristics we return to the photoemission results. As mentioned above, the highest EWF values were obtained when interfacial BDMT was present (4.05-4.0 eV), followed by interfaces without additive (3.6-4.0 eV), and the lowest values with interfacial HEG-DT (3.5-3.7 eV). According to these values, the interfacial energy level alignment for electron transfer from PCBM to the contact will be best for interfaces with HEG-DT, followed by interfaces without additive, and lowest for interfacial BDMT. This trend is in agreement with the device characteristics in this study, as V_{oc} and FF of devices with HEG-DT interlayers are higher than those of devices with no interlayer, while V_{oc} and FF of devices with BDMT interlayers are lower than those of devices with no interlayer. As expected, metal work function values are insufficient to predict the interfacial energy level alignment at the buried interfaces. Rather, the contribution of an interlayer should be estimated by comparing EWF values of a specific organic/metal interface with and without the interlayer.

Next, we turn to investigating the effect of additive concentration on EWF and device characteristics. It was previously shown that the extent of work function modification by depositing dipole layers on a metal surface depends linearly on the projection and area density of the dipole moments.[4, 37] Under such conditions, the work function modification will increase with layer coverage until a saturation value will be reached at full coverage. We speculate that EWF evolution with the amount of additives at the buried interface follows a similar trend. Namely, additive molecules reaching the organic/metal interface impose a local modification of the EWF that increases until full coverage is obtained and EWF saturates at the value measured in Figure 3. EWF evolution with additive concentration at the interface will lead to a similar evolution of V_{oc}. Indeed, Figure 4c and Tables 1 and 2 show that for both HEG-DT and BDMT additives there is a progressive evolution of V_{oc} with additive concentration.

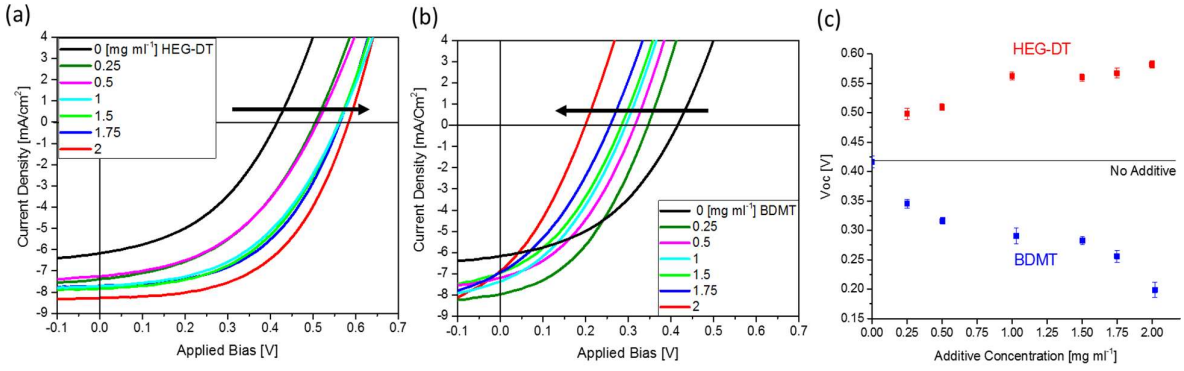

Figure 4: Average J-V curves under illumination of P3HT:PCBM OSC devices with different concentration of (a) HEG-DT; and (b) BDMT. (c) V_{oc} of the same devices shown in (a) and (b) as a function of additive concentration.

Table 1: Average performance values of the OSC devices with concentration series of HEG-DT

HEG-DT content [mg ml^{-1}]	V_{oc} [v]	J_{sc} [mA cm^{-2}]	FF	PCE [%]
0	0.42 ± 0.01	6.17 ± 0.36	0.42 ± 0.02	1.09 ± 0.12
0.25	0.50 ± 0.01	7.35 ± 0.64	0.42 ± 0.01	1.55 ± 0.12
0.5	0.51 ± 0.01	7.26 ± 0.69	0.45 ± 0.01	1.67 ± 0.10
1	0.56 ± 0.01	7.71 ± 0.58	0.48 ± 0.01	2.10 ± 0.09
1.5	0.56 ± 0.01	7.82 ± 0.81	0.49 ± 0.01	2.16 ± 0.19
1.75	0.57 ± 0.01	7.45 ± 0.66	0.52 ± 0.01	2.21 ± 0.18
2	0.58 ± 0.01	8.27 ± 1.05	0.54 ± 0.01	2.57 ± 0.28

Table 2: Average performance values of the OSC devices with concentration series of BDMT

BDMT content [mg ml^{-1}]	V_{oc} [v]	J_{sc} [mA cm^{-2}]	FF	PCE [%]
0	0.42 ± 0.01	6.17 ± 0.36	0.42 ± 0.02	1.09 ± 0.12
0.25	0.34 ± 0.01	7.97 ± 0.73	0.41 ± 0 .01	1.13 ± 0.08
0.5	0.32 ± 0.01	7.19 ± 0.71	0.39 ± 0.01	0.90 ± 0.08
1	0.29 ± 0.01	7.17 ± 0.57	0.37 ± 0.01	0.76 ± 0.05
1.5	0.28 ± 0.01	7.26 ± 0.80	0.35 ± 0.01	0.71 ± 0.10
1.75	0.26 ± 0.01	6.93 ± 0.43	0.34 ± 0.01	0.61 ± 0.05
2	0.20 ± 0.01	6.87 ± 0.68	0.32 ± 0.01	0.44 ± 0.07

This journal is © The Royal Society of Chemistry 20xx

The suggested mechanism for the evolution of EWF with additive interfacial concentration is corroborated by generating mixed HEG-DT and BDMT interlayers. To do so, appropriate amounts of HEG-DT and BDMT mixtures were blended into the active layer of the P3HT:PCBM-based OSCs. The overall concentration of additives was kept constant while the composition of the additive mixture ranged from HEG-DT-only to BDMT-only. We note that the additives do not necessarily have the same diffusion coefficient due to their different properties including size, surface energy, and interactions with the bottom substrate and organic BHJ components. The averaged J-V curves under illumination and corresponding V_{oc} trends as a function of additive mixture composition are presented in Figure 5a and b, respectively. The performance details of the OSC devices are presented in table 3. Averaged J-V curves in the dark and comparison of photovoltaic parameters for devices with additives and additive mixtures are presented in the supplementary information Figures S2 and S3, respectively.

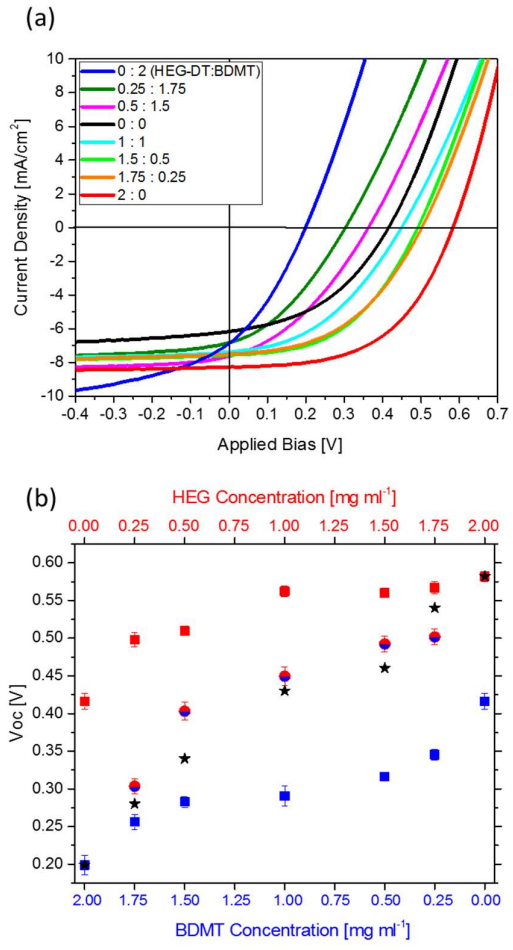

Figure 5: Average J-V curves under illumination of P3HT:PCBM (20:20 mg ml^{-1}) OSC devices with mixtures of HEG-DT:BDMT additives. The inset lists the composition of additive mixture in [mg ml^{-1}] so that the overall concentration of additives is 2 mg ml^{-1}. (b) Voc as a function of type and concentration of additives and additive mixtures. The red symbols and top x-axis correspond to HEG-DT alone, while the blue symbols and bottom x-axis correspond to BDMT only. The mixed red/blue symbols represent Voc values of devices prepared with additive mixtures and the black stars are values calculated for the same mixtures using equation 1.

Figure 5 clearly shows that introducing additive mixtures to the BHJ sensitively tunes the V_{oc} between the values obtained for each of the pure additives (blue and red squares in Figure 5b). This result confirms migration of both additives towards the silver electrode during its deposition to form a mixed interlayer. The local EWF modulation by the additives is cumulative and the overall interfacial EWF across the interface is a sum of the local EWF modulations. Under such conditions, the EWF and V_{oc} can be quantitatively estimated from the values obtained for each additive and a simple blend law equation:

$$V_{oc}^{mixture} = W_{HEG-DT} \cdot V_{oc}^{C_{HEG-DT}} + W_{BDMT} \cdot V_{oc}^{C_{BDMT}}$$

Where the $V_{oc}^{C_{Additive}}$ is the V_{oc} value obtained for devices with additive concentration $C_{additive}$. $W_{additive}$ is the weight percent of that additive in the blend. The calculated values are shown as black stars in Figure 5b and exhibit a similar trend as the experimental V_{oc} values. The similar behaviour indicates that indeed the overall EWF, and hence V_{oc}, are sensitively tuned by the sum of the local EWF values at the interface. The calculated V_{oc} values are generally lower than the experimental ones, reflecting a slightly higher relative concentration of HEG-DT at the interface compared to that in the mixture. The latter might be associated with easier diffusion of HEG-DT through the BHJ, compared to that of BDMT, despite of HEG-DT's higher molecular weight. We suggest that interactions between the phenyl ring of BDMT and the BHJ components stalls its migration, while the ether character of HEG-DT allows it to migrate faster to the electrode.

Finally, Raman measurements were performed to study the effect of the self-generated interlayers on the chemical environment of the buried interface. To do that, we employed Surface Enhanced Resonance Raman Spectroscopy (SERRS), which allows selective probing of the conformation of polymer chains close to the interface between silver and organic layer. The silver plasmon resonance that is generated from the excitation enhances the electric field in the vicinity of the metal and, as a result, the Raman signal of any molecule within 10 nm from the metal surface is enhanced.[38] Further enhancement of the signal is achieved by selecting the excitation wavelength to be in resonance with an electronic transition of the polymer of interest. In this case, excitation at 473 nm was chosen to both probe effectively the P3HT component of the examined films and to enable plasmon resonance with the silver. At this excitation wavelength only highly Raman-active vibrational bands of the polymer are observed. For insight on the conformation of the P3HT chains we follow the thiophene ring C-C (1380 cm^{-1}) and C=C (1450 cm^{-1}) symmetric stretch modes, from which the degree of P3HT torsional conformation, i.e. planarity, can be estimated.[39, 40] Increased intensity of the C-C stretch relative to that of the C=C mode, and a shift of the C=C band to lower frequencies have been previously assigned to increased planarity between monomer units due to better electron cloud delocalization.[39]

Table 3: Average performance of the OSC device with concentration series of HEG-DT:BDMT intermix

HEG-DT:BDMT content [mg ml^{-1}]	V_{oc} [v]	J_{sc} [mA cm^{-2}]	FF	PCE [%]
0.25:1.75	0.42 ± 0.01	6.17 ± 0.36	0.42 ± 0.02	1.09 ± 0.12
0.5:1.5	0.34 ± 0.01	7.97 ± 0.73	0.41 ± 0 .01	1.13 ± 0.08
1:1	0.32 ± 0.01	7.19 ± 0.71	0.39 ± 0.01	0.90 ± 0.08
1.5:0.5	0.29 ± 0.01	7.17 ± 0.57	0.37 ± 0.01	0.76 ± 0.05
1.75:0.25	0.50 ± 0.01	7.50 ± 0.43	0.46 ± 0.01	1.74 ± 0.08

The conformation of P3HT chains at the organic/Ag buried interface, with and without additive interlayers, is studied by depositing P3HT and P3HT:PCBM films with and without additives on glass substrates with thin Ag layers. The SERRS spectra in Figure 6 clearly show that the additives induce changes to the Raman spectra of P3HT with respect to neat films of P3HT and P3HT:PCBM. Both HEG-DT and BDMT induce a narrowing of the C=C stretch mode in P3HT, centred at 1450 cm^{-1}, along with an increased intensity of the C-C stretch, indicating an improved planarity of the P3HT chains compared to the P3HT polymer alone or in the BHJ blend (green and black lines in Figure 6, respectively), where in the P3HT:PCBM BHJ case, the band is shifted towards higher frequencies (1470 cm^{-1}) due to torsionally disordered chains.[39] The SERRS results reveal that, as expected, blending PCBM with P3HT increases the disorder of the P3HT chains on the molecular-level.[39-41] The disorder of P3HT by PCBM measured here is more significant than in previous reports probably due to the vertical segregation of PCBM to the bottom interface.[38] However, when incorporating additives, a significant enhancement of P3HT chain-planarity is induced, which occurs both in the bulk of the film (supplementary information Figure S4) and at the organic/metal interface. This effect is present only when the additives are blended into the organic film and not when deposited as a separate layer (Supplementary Information Figure S4). The enhancement of chain planarity can potentially facilitate charge transport through inter-chain interactions. However, the fact that both additives direct similar polymer chain conformation at the interface, while one increases and one reduces V_{oc}, demonstrates that V_{oc} modification in this study goes beyond polymer conformation and ordering. We therefore conclude that V_{oc} modification is a result of interfacial EWF generated by formation of the interlayers at the buried organic/metal interface.

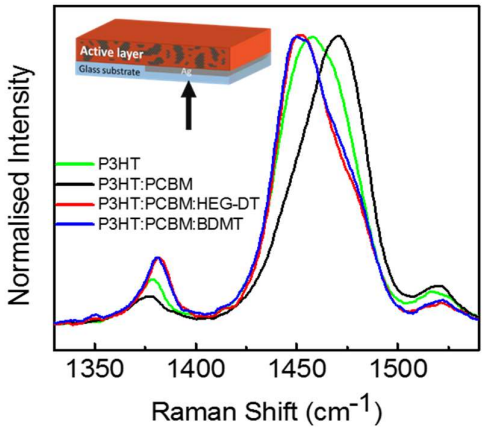

Figure 6: Surface enhanced resonance Raman spectra of P3HT at the Ag/organic interface. SERRS of neat P3HT (green), P3HT:PCBM (black), and P3HT:PCBM mixed with 5 [mg ml^{-1}] additive of HEG-DT (red) or BDMT (blue). The Inset shows a schematic illustration of the SERRS measurement conditions.

Conclusions

In this study we used self-generated interlayers in OSC to provide insight on the energy level alignment at the organic semiconductor/back contact interface, with and without interlayers, and its effect on V_{oc} and FF. We highlight that instead of electrode work function rather the interfacial EWF reflects the energy level alignment more accurately. Measuring EWF of the buried interface is generally not possible, but its value can be estimated by comparing the EWF of metal sequentially deposited onto a thin additive layer and that of additive layer formed directly on metal thin films. In this way, each interlayer/metal interface in constructed in two opposing ways, which indeed allows assessing plausible EWF values, provided that the metal overlayers are not too thick and continuous. To understand the contribution of each back contact interlayer to device characteristics, the interlayer/metal EWF should be compared to the EWF value of the same BHJ/back contact interface without interlayer. This methodology should replace the common approach that estimates the contribution of an interlayer by comparing the work function of the metal contact with and without an interlayer. In the case of interlayers self-generated by additive migration, the EWF evolves with interlayer formation. The EWF modification is local and cumulative so that the overall interfacial EWF across the interface is a sum of the local EWF modulations and saturates at full interlayer coverage. Accordingly, EWF, and hence V_{oc}, can be sensitively tuned using interlayers composed of additive mixtures. It is also important to note that additive migration to the organic/metal interface could modify BHJ bulk and interfacial morphologies. However, the significant effect of interlayer formation on device characteristics is not assigned to these morphology changes but rather to the energy level alignment imposed by the interlayer.

Conflicts of interest

There are no conflicts to declare.

This journal is © The Royal Society of Chemistry 20xx

Please do not adjust margins

Acknowledgements

This research was supported by a grant from the German-Israeli Foundation (GIF) for Scientific Research and Development and the European Union's Horizon 2020 research and innovation programme under the Marie Sklodowska-Curie grant agreement No 675867. BS wishes to thank the Israel Ministry of Science for a doctoral fellowship.

References

1. L. Lucera, F. Machui, P. Kubis, H. D. Schmidt, J. Adams, S. Strohm, T. Ahmad, K. Forberich, H. J. Egelhaaf and C. J. Brabec, *Energy & Environmental Science*, 2016, **9**, 89-94.
2. H. Youn, H. J. Park and L. J. Guo, *Small*, 2015, **11**, 2228-2246.
3. E. Bundgaard and F. C. Krebs, *Solar Energy Materials and Solar Cells*, 2007, **91**, 954-985.
4. N. Koch, *physica status solidi (RRL) – Rapid Research Letters*, 2012, **6**, 277-293.
5. Y. Gao, *Materials Science and Engineering: R: Reports*, 2010, **68**, 39-87.
6. N. Koch, *ChemPhysChem*, 2007, **8**, 1438-1455.
7. A. Kahn, N. Koch and W. Gao, *Journal of Polymer Science Part B: Polymer Physics*, 2003, **41**, 2529-2548.
8. A. Guerrero, B. Dörling, T. Ripolles-Sanchis, M. Aghamohammadi, E. Barrena, M. Campoy-Quiles and G. Garcia-Belmonte, *ACS Nano*, 2013, **7**, 4637-4646.
9. T.-H. Lai, S.-W. Tsang, J. R. Manders, S. Chen and F. So, *Materials Today*, 2013, **16**, 424-432.
10. E. L. Ratcliff, B. Zacher and N. R. Armstrong, *The Journal of Physical Chemistry Letters*, 2011, **2**, 1337-1350.
11. L.-M. Chen, Z. Xu, Z. Hong and Y. Yang, *Journal of Materials Chemistry*, 2010, **20**, 2575-2598.
12. T. M. Khan, Y. Zhou, A. Dindar, J. W. Shim, C. Fuentes-Hernandez and B. Kippelen, *ACS Applied Materials & Interfaces*, 2014, **6**, 6202-6207.
13. B.-H. Jiang, Y.-J. Peng and C.-P. Chen, *Journal of Materials Chemistry A*, 2017, **5**, 10424-10429.
14. E. L. Ratcliff, A. Garcia, S. A. Paniagua, S. R. Cowan, A. J. Giordano, D. S. Ginley, S. R. Marder, J. J. Berry and D. C. Olson, *Advanced Energy Materials*, 2013, **3**, 647-656.
15. S. Braun, W. R. Salaneck and M. Fahlman, *Advanced Materials*, 2009, **21**, 1450-1472.
16. R. Steim, F. R. Kogler and C. J. Brabec, *Journal of Materials Chemistry*, 2010, **20**, 2499-2512.
17. P. Cheng and X. Zhan, *Chemical Society Reviews*, 2016, **45**, 2544-2582.
18. M. O. Reese, M. S. White, G. Rumbles, D. S. Ginley and S. E. Shaheen, *Applied Physics Letters*, 2008, **92**, 053307.
19. I. Deckman, M. Moshonov, S. Obuchovsky, R. Brener and G. L. Frey, *Journal of Materials Chemistry A*, 2014, **2**, 16746-16754.
20. B. Shamieh, S. Obuchovsky and G. L. Frey, *Journal of Materials Chemistry C*, 2016, **4**, 1821-1828.
21. J. Vinokur, B. Shamieh, I. Deckman, A. Singhal and G. L. Frey, *Chemistry of Materials*, 2016, **28**, 8851-8870.
22. J. Vinokur, S. Obuchovsky, I. Deckman, L. Shoham, T. Mates, M. L. Chabinyc and G. L. Frey, *ACS Applied Materials & Interfaces*, 2017, **9**, 29889-29900.
23. I. Deckman, S. Obuchovsky, M. Moshonov and G. L. Frey, *Langmuir*, 2015, **31**, 6721-6728.
24. W. Qingshuo, N. Takeshi, T. Keisuke and H. Kazuhito, *Advanced Materials*, 2008, **20**, 2211-2216.
25. I. Hisao, S. Kiyoshi, I. Eisuke and S. Kazuhiko, *Advanced Materials*, 1999, **11**, 605-625.
26. S. M. P. and D. W. A., *Surface and Interface Analysis*, 1979, **1**, 2-11.
27. H. Zhu and R. Ramprasad, *Physical Review B*, 2011, **83**, 081416.
28. A. Guerrero, L. F. Marchesi, P. P. Boix, S. Ruiz-Raga, T. Ripolles-Sanchis, G. Garcia-Belmonte and J. Bisquert, *ACS Nano*, 2012, **6**, 3453-3460.
29. K. Murty, M. Venkataramanan and T. Pradeep, *Langmuir*, 1998, **14**, 5446-5456.
30. J. Kubackova, I. Izquierdo-Lorenzo, D. Jancura, P. Miskovsky and S. Sanchez-Cortes, *Physical Chemistry Chemical Physics*, 2014, **16**, 11461-11470.
31. L. Salazar Alarcón, L. J. Cristina, J. Shen, J. Jia, V. A. Esaulov, E. A. Sánchez and O. Grizzi, *The Journal of Physical Chemistry C*, 2013, **117**, 17521-17530.
32. T. Aqua, H. Cohen, O. Sinai, V. Frydman, T. Bendikov, D. Krepel, O. Hod, L. Kronik and R. Naaman, *The Journal of Physical Chemistry C*, 2011, **115**, 24888-24892.
33. J.-P. Hong, A.-Y. Park, S. Lee, J. Kang, N. Shin and D. Y. Yoon, *Applied Physics Letters*, 2008, **92**, 131.
34. M. Oehzelt, N. Koch and G. Heimel, *Nature Communications*, 2014, **5**, 4174.
35. R. Smoluchowski, *Physical Review*, 1941, **60**, 661-674.
36. N. D. Lang and W. Kohn, *Physical Review B*, 1971, **3**, 1215-1223.
37. Y. Zhou, C. Fuentes-Hernandez, J. Shim, J. Meyer, A. J. Giordano, H. Li, P. Winget, T. Papadopoulos, H. Cheun, J. Kim, M. Fenoll, A. Dindar, W. Haske, E. Najafabadi, T. M. Khan, H. Sojoudi, S. Barlow, S. Graham, J.-L. Brédas, S. R. Marder, A. Kahn and B. Kippelen, *Science*, 2012, **336**, 327-332.
38. J. Razzell-Hollis, Q. Thiburce, W. C. Tsoi and J.-S. Kim, *ACS Applied Materials & Interfaces*, 2016, **8**, 31469-31481.
39. W. C. Tsoi, D. T. James, J. S. Kim, P. G. Nicholson, C. E. Murphy, D. D. C. Bradley, J. Nelson and J.-S. Kim, *Journal of the American Chemical Society*, 2011, **133**, 9834-9843.
40. Y. Gao, T. P. Martin, E. T. Niles, A. J. Wise, A. K. Thomas and J. K. Grey, *The Journal of Physical Chemistry C*, 2010, **114**, 15121-15128.
41. J. Razzell-Hollis, W. C. Tsoi and J. S. Kim, *Journal of Materials Chemistry C*, 2013, **1**, 6235-6243.

This journal is © The Royal Society of Chemistry 20xx

Please do not adjust margins